Advanced EPR

Applications in Biology and Biochemistry

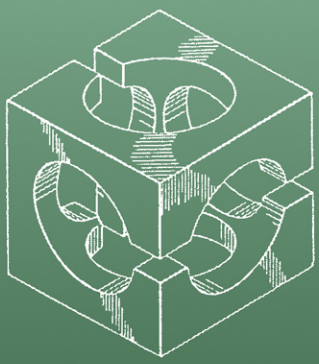

Edited by

A.J. Hoff

Elsevier

Advanced EPR

Applications in Biology and Biochemistry

This page intentionally left blank

Advanced EPR

Applications in Biology and Biochemistry

Edited by

A.J. Hoff

Huygens Laboratory, State University of Leiden,
Niels Bohrweg 2, P.O. Box 9504, 2300 RA Leiden,
The Netherlands

ELSEVIER

Amsterdam – Oxford – New York – Tokyo 1989

ELSEVIER SCIENCE PUBLISHERS B.V.
Sara Burgerhartstraat 25
P.O. Box 211, 1000 AE Amsterdam, The Netherlands

Distributors for the United States and Canada:

ELSEVIER SCIENCE PUBLISHING COMPANY INC.
655, Avenue of the Americas
New York, NY 10010, U.S.A.

ISBN 0-444-88050-X

Printed in The Netherlands

Dedicated to George Feher on the occasion of his 65th birthday, in recognition of his seminal work on the development of EPR and ENDOR and their application to biological systems.

This page intentionally left blank

PREFACE

In 1945 E. Zavoisky published the first electron paramagnetic resonance experiment, the first successful magnetic resonance experiment ever [Fiz. Zh.,9(1945)211–245]. Three decades later, EPR had reached full maturity. So much so that a decline appeared to set in and many chemistry departments, regarding EPR primarily as an analytic tool, shifted their research effort in spectroscopy to other techniques. Only in a few niches EPR still flourished, and it is truly amazing that we are now witnessing such a strong revival. This, in my opinion, is due to two prime causes: Firstly, applications of EPR and, parallel with it, electron-nuclear double resonance in biology and biochemistry, although started early enough, had a much longer incubation time than those in chemistry and only now appear to have entered an exponential growth phase. Secondly, about ten years ago pulsed EPR techniques, albeit devised two decades earlier, began to take off with the general availability of low-cost microwave switches and solid-state amplifiers and with the development of special cavities. The penetration of EPR into biological research and the development of new techniques have lead to, and are the result of, the founding of several EPR centers devoted to the biological applications of EPR and ENDOR. This in turn has led to a rather spectacular growth in the number of applications in which advanced EPR techniques are used to tackle problems of biological interest.

From the above it will be clear, I think, that now is a particularly propitious time to publish a book reporting on the new developments in EPR and ENDOR, with emphasis on applications in biology and biochemistry. The present volume is broadly organized into four parts. In Chapters 1–6 pulsed EPR is discussed in detail. Peisach and Mims give a general introduction to Electron Spin Echo (ESE) and Electron Spin Echo Envelop Modulation (ESEEM) spectroscopy, pointing out their capabilities and pitfalls and reviewing applications primarily in metalloenzyme studies. Dikanov and Astashkin discuss ESEEM of disordered systems in depth, emphasizing simple, approximate relations for extracting information on hyperfine and quadrupole couplings and on the number and geometry of coupled nuclei, while Singel describes the advantages of multi-frequency ESEEM. De Beer and van Ormondt give a thorough and much needed treatment of recent sophisticated mathematical techniques for resolution enhancement in the time-domain analysis of ESEEM. Freed and coworkers give a detailed account of Fourier-transform ESE and of 2D-ESE and -ELDOR (electron-electron double resonance), with applications to nitroxide spin labels, from which it is clear that EPR now approaches the sophistication of NMR techniques. Schweiger reviews a number of his novel schemes for pulsed EPR and ENDOR, which allow higher selectivity and time resolution than the standard techniques.

In the second part of the book Chapters 7–12 provide detailed discussions of a number of novel experimental methods. Hyde and Froncisz treat the design of a variety of loop-gap resonators and their applications, including cw and pulsed EPR, ENDOR and *in situ* electrochemical generation of radicals. The construction and applications of a very high frequency (250 GHz) cw-EPR spectrometer is described by Freed and coworkers. A paper by Feher and coworkers (reprinted with permission of the American Institute of Physics) calls attention to the method of temperature modulation, a technique that, although presently seldom utilized, is nevertheless eminently useful for the registrationof very broad lines of, for example, metalloproteins. In three chapters, McLauchlan and Stehlik and coworkers review the theory and applications of time-resolved and transient-nutation EPR while Hore discusses the detailed analysis of spin-polarized spectra recorded with these two techniques.

The third part of the book sees seven chapters on double-resonance techniques, five on ENDOR and two on optically- and reaction yield-detected resonance. Möbius and coworkers give a detailed account of ENDOR and TRIPLE resonance of radicals in liquid solution with emphasis on photosynthetic pigments and reaction centers. Hoffman and coworkers introduce the theory of solid state ENDOR and describe its application to the study of metalloproteins, except hemoglobin, which is treated by Kappl and Hüttermann. Brustolon and Segre describe ENDOR of disoriented systems, with applications to nitroxide spin labels, while Dinse discusses the exciting possibilities of pulsed ENDOR. The editor of this book reviews ODMR with emphasis on the applications to biochemistry and especially photosynthesis, whereas the theory and applications of RYDMR are outlined by Lersch and Michel-Beyerle.

The fourth and final part of the book is devoted to a thorough discussion of a number of new developments in the application of EPR to various biological and biochemical problems. Marsh and Horvath treat the modern, refined methods of the simulation of the spectra of nitroxide spin labels, incorporated in lipid membranes under different regimes of motion. Swartz and Glockner introduce the use of spin labels for the measurement of the concentration of oxygen in cells and tissue and give a few examples of the fascinating possibilities of EPR-imaging. Hagen discusses his breakthrough work on g-strain broadening of metalloproteins. Moura et al. review their and others' extensive work on a variety of iron-sulfur proteins, native and with substituted Fe-clusters. Brudvig treats EPR spectroscopy of Mn-proteins, culminating in a description of the work done on the oxygen-evolving complex of plant photosynthesis. Finally, in the last chapter, Solomon and coworkers give a comprehensive account of the spectroscopy of copper proteins, interrelating EPR and ENDOR with a number of other spectroscopic techniques.

The present volume is, I believe, not only an up-to-date survey of existing EPR techniques and their applications in biology and biochemistry, but also gives many ideas for future developments in instrumentation and theory. It is clear that the future of pulsed EPR is very bright indeed, and extension to other frequencies, both lower and (much) higher than 9 GHz, has been achieved or is underway. New microwave-bridge and cavity designs are revolutionizing the EPR spectrometer. Very high frequency cw-EPR is an extremely promising tool for biochemical and biophysical studies. The development of the theory of spin-label EPR in all motional regimes and of g-strain broadening goes hand-in-hand with tremendous advances in data reduction and simulation algorithms. The field is alive and lively indeed and we owe the contributors much for communicating so well a sense of wonder and expectation.

The figures in this volume are original or are reproduced with the permission of the author and copyright holder. I am indebted to the American Institute of Physics for permission to reproduce an article by Feher et al. (Chapter 9). I am grateful to all authors for consenting to submit camera-ready manuscripts, even if this meant spending hours trying to induce refractive word-processing equipment to cooperate. This has reduced the production costs of the book considerably. All have made a real effort to make the presentation of the various chapters as uniform as possible and, although overlap in a multi-author volume is to some extent inevitable and even useful, to avoid unnecessary duplication by cross-referencing to related chapters.

Last but not least, I acknowledge a special debt to Zina for allowing me to sacrifice so many hours to the preparation of this book that would have been better spent bicycling with her through the tulip fields around Leiden. Through Zina I salute all authors' partners for their support.

A.J. Hoff Leiden, May 1989

CONTENTS

LIST OF CONTRIBUTORS

A.V. Astashkin	Institute of Chemical Kinetics and Combustion, Academy of Sciences of the USSR, Novosibirsk 630090, U.S.S.R.
C.H. Bock	Fachbereich Physik, Freie Universität Berlin, Arnimallee 14, D-1000 Berlin 33, B.R.D.
G.W. Brudvig	Department of Chemistry, Yale University, New Haven, CT 06511, U.S.A.
M. Brustolon	Dipartimento di Chimica Fisica, Università di Padova, Via Loredan 2, I-35131 Padova, Italy
D.E. Budil	Department of Chemistry, Cornell University, Ithaca, NY 14853, U.S.A.
R. de Beer	Department of Applied Physics, University of Technology, P.O. Box 5046, 2600 GA Delft, The Netherlands
S.A. Dikanov	Institute of Chemical Kinetics and Combustion, Academy of Sciences of the USSR, Novosibirsk 630090, U.S.S.R.
K.-P. Dinse	Institut für Physik, Universität Dortmund, Otto Hahnstrasse 30, D-4600 Dortmund 50, B.R.D.
K.A. Earle	Department of Chemistry, Cornell University, Ithaca, NY 14853, U.S.A.
G. Feher	Department of Chemistry, University of California - San Diego, La Jolla, CA 92093, U.S.A.
J.H. Freed	Department of Chemistry, Cornell University, Ithaca, NY 14853, U.S.A.

W. Froncisz	Department of Biophysics, National Biomedical ESR Center, Medical College of Wisconsin, Milwaukee, WI 53226, U.S.A.
A.A. Gewirth	Department of Chemistry, Stanford University, Stanford, CA 94305-5080, U.S.A.
J.F. Glockner	College of Medicine, University of Illinois, 190 Medical Sciences Building, 506 S. Mathews Avenue, Urbana, IL 61801, U.S.A.
J. Gorcester	Rijksuniversiteit Leiden, Huygens Laboratorium, Niels Bohrweg 2, Postbus 9504, 2300 RA Leiden, The Netherlands
R.J. Gurbiel	Institute of Molecular Biology, Jagiellonian University, al. Mickiewicza 3, 31-120 Krakow, Poland
W.R. Hagen	Department of Biochemistry, Agricultural University, Dreijenlaan 3, 6703 HA Wageningen, The Netherlands
A.J. Hoff	Department of Biophysics, Huygens Laboratory, State University of Leiden, P.O. Box 9504, 2300 RA Leiden, The Netherlands
B.M. Hoffman	Department of Chemistry, Northwestern University, Evanston, IL 60201, U.S.A.
P.J. Hore	Physical Chemistry Laboratory, Oxford University, Oxford OX1 3QZ, England
L.I. Horváth	Institute of Biophysics, Biological Research Centre, H-6701 Szeged, Hungary
J. Hüttermann	Biophysik und Physikalische Grundlagen der Medizin, Universität des Saarlandes, D-6650 Homburg/Saar, B.R.D.

J.S. Hyde	Department of Biophysics, National Biomedical ESR Center, Medical College of Wisconsin, Milwaukee, WI 53226, U.S.A.
R.A. Isaacson	Department of Chemistry, University of California - San Diego, La Jolla, CA 92093, U.S.A.
R. Kappl	Biophysik und Physikalische Grundlagen der Medizin, Universität des Saarlandes, D-6650 Homburg/Saar, B.R.D.
W. Lersch	Institut für Physikalische und Theoretische Chemie der Technischen Universität München, Lichtenbergstrasse 4, D-8046 Garching, B.R.D.
W. Lubitz	Physikalisches Institut, Universität Stuttgart, Teilinstitut 2, Pfaffenwaldring 57, D-7000 Stuttgart 80, B.R.D.
W.B. Lynch	Advanced Materials Corp., c/0 Mellon Institute, 4400 Fifth Avenue, Pittsburgh, PA 15213, U.S.A.
A. Macedo	Centro de Qulmica Estrutural, Complexo Interdisciplinar, Av. Rovisco Pais - 1096 Lisboa Codex, Portugal
D. Marsh	Max-Planck-Institut für Biophysikalische Chemie, Abteiling Spektroskopie, D-3400 Göttingen, B.R.D.
J.D. McElroy	AT&T Bell Laboratories, 260 Cherry Hill Road, Parsippany, NJ 07054, U.S.A.
K.A. McLauchlan	Physical Chemistry Laboratory, University of Oxford, South Parks Road, Oxford OX1 3QZ, England
M.E. Michel-Beyerle	Institut für Physikalische und Theoretische Chemie der Technischen Universität München, Lichtenbergstrasse 4, D-8046 Garching, B.R.D.

G.L. Millhauser	Department of Chemistry, University of California, Santa Cruz, CA 95064, U.S.A.
W.B. Mims	Exxon Research and Engineering Company, Annandale, NJ 08801, U.S.A.
K. Möbius	Institut für Molekülphysik, Fachbereich Physik, Freie Universität Berlin, Arnimallee 14, D-1000 Berlin 33, B.R.D.
I. Moura	Centro de Química Estrutural, Complexo Interdisciplinar, Av. Rovisco Pais - 1096 Lisboa Codex, Portugal
J.J.G. Moura	Centro de Química Estrutural, Complexo Interdisciplinar, Av. Rovisco Pais - 1096 Lisboa Codex, Portugal
J. Peisach	Departments of Molecular Pharmacology and Physiology and Biophysics, Albert Einstein College of Medicine, 1300 Morris Park Avenue, Bronx, NY 10461, U.S.A.
M. Plato	Institut für Molekülphysik, Fachbereich Physik, Freie Universität Berlin, Arnimallee 14, D-1000 Berlin 33, B.R.D.
A. Schweiger	Laboratory of Physical Chemistry, Swiss Federal Institute of Technology, ETH-Zentrum, CH-8092 Zurich, Switzerland
U. Segre	Dipartimento di Chimica Fisica, Università di Padova, Via Loredan 2, I-35131 Padova, Italy
D.J. Singel	Department of Chemistry, Harvard University, 12 Oxford Street, Cambridge, MA 02138, U.S.A.
M. Sivaraja	Department of Chemistry, Northwestern University, Evanston, IL 60201, U.S.A.

E.I. Solomon	Department of Chemistry, Stanford University, Stanford, CA 94305-5080, U.S.A.
D. Stehlik	Fachbereich Physik, Freie Universität Berlin, Arnimallee 14, D-1000 Berlin 33, B.R.D.
H.M. Swartz	College of Medicine, University of Illinois, 190 Medical Sciences Building, 506 S. Mathews Avenue, Urbana, IL 61801, U.S.A.
M.C. Thurnauer	Chemistry Division, Argonne National Laboratory, 9700 South Cass Avenue, Argonne, IL 60439, U.S.A.
D. van Ormondt	Department of Applied Physics, University of Technology, P.O. Box 5046, 2600 GA Delft, The Netherlands
M.M. Werst	Department of Chemistry, Northwestern University, Evanston, IL 60201, U.S.A.
T.D. Westmoreland	Department of Chemistry, Stanford University, Stanford, CA 94305-5080, U.S.A.

This page intentionally left blank

CHAPTER 1

ESEEM AND LEFE OF METALLOPROTEINS AND MODEL COMPOUNDS*

WILLIAM B. MIMS and JACK PEISACH

1. INTRODUCTION

It is surprising, perhaps, that experiments which involve coherent excitation should have played such a minor role in EPR, all the more so since the sources of excitation used in EPR have always been coherent, obviating any need for developing a new kind of signal source as in coherent optics. The reason, on closer examination, lies in the short intrinsic coherence times of the physical systems examined by the microwave resonance method, and in the excess broadening of many resonance lines caused by crystal strains. At low temperatures, where lattice relaxation times cease to affect linewidth, this excess broadening or inhomogeneous broadening, still often produces linewidths of the order of 10 G (28 MHz), even in the ideal case of lightly doped, single crystal samples. In the time domain this corresponds to a lifetime of 11 nanoseconds.

Fortunately, the spin echo technique provides a means of overcoming inhomogeneous line broadening, and by using this method one can observe spin coherence for times of several microseconds, or more. In the frequency domain this corresponds to a linewidth of less than 0.03 MHz or 10 milligauss. The electron spin coherence times, or phase memory times, remain several microseconds, even in crystalline samples with very broad inhomogeneous lines, or in frozen solution samples where the EPR spectrum consists of a continuum, many hundreds of gauss wide. The technical price for making use of this convenient property is the acquisition of a short-pulse, high-power microwave transmitter system, a low-noise, non-overloading receiver, and a timing and pulse programming system. All but the first of these are becoming cheaper and more readily available, and thirty or more laboratories world-wide are now equipped to perform coherent EPR experiments of this kind (1).

Coherent EPR methods have been found especially useful for investigating materials that are not available in single crystal form. The very broad spectral distributions found in powders and frozen solutions pose no new problems, other than those of signal intensity, since the coherence times are

*This work was supported in part by Grants RR-02583 and GM-40168 from the United States Public Health Service.

no shorter, and the corresponding spectral widths, or "spin packet" widths, are not greater than in single crystals. Such methods would indeed seem to be intrinsically destined to find a major application in metalloprotein studies. Several different types of coherent EPR experiments have been proposed, but, out of these only two have found a biological application, and they will form the subject of this article. A third type of experiment, pulsed ENDOR in its several forms (see the Chapter by K.P. Dinse), has been performed on non-biological materials and may be expected to find a biological application in the future.

The first method to be discussed here, the electron spin echo envelope modulation (ESEEM) method, forms a natural complement to ENDOR, either in its non-coherent continuous wave mode or in its pulsed mode. The ESEEM method is particularly well suited for detecting nuclei that are weakly coupled to nearby electrons -- for example the nuclei of a ligand atom or of a substrate atom in a metalloprotein complex. Since this appears to be a promising field of application, we shall spend much time discussing ways of performing this kind of experiment. For more general discussions of ESEEM as a spectroscopic tool, reference can be made to review articles in this (the Chapters by S.A. Dikanov and D. Singel) and in other volumes (2-5).

The second method to be discussed here is based on a measurement of the linear electric field effect (LEFE) in EPR, which is useful for investigating the symmetry and bonding of paramagnetic complexes. Although there have been numerous LEFE experiments performed on inorganic single crystal samples, this method has been used on metalloprotein samples only by the authors of the present article, who offer apologies here for constant references to their own work. The paucity of LEFE work in the biological area is due to the fact that a short-pulse, high-power pulsed EPR system is indispensable for LEFE measurements on metalloprotein samples in frozen solution, whereas older, non-coherent continuous wave methods are, to a certain degree, successful with inorganic single crystals. We should like to stress the fact that any laboratory already possessing a short-pulse electric spin echo (ESE) system -- for example, an instrument acquired in order to perform ESEEM studies -- can, for several thousand dollars and some extra shop work, gain access to the LEFE method. Although LEFE measurements may be needed only occasionally to answer some particular questions, the investment would seem to be worthwhile, and we hope that the present review may encourage laboratories possessing ESE equipment to take the necessary upgrading step. Some practical details regarding LEFE techniques are found in reference (6). Earlier review articles dealing generally with the application of ESE techniques related to biological materials are in refs. 2-5.

2. APPLICATION INVOLVING THE NUCLEAR MODULATION EFFECT (ESEEM)

The electron spin echo envelope modulation (ESEEM) effect is described in detail elsewhere in this volume. We can, therefore, confine ourselves here to stating the essential formulae and to outlining those features which bear directly on the application of ESEEM measurements to the study of metal-ion-ligand complexes, such as those encountered in metalloprotein samples and in model compounds.

The modulation effect arises as a result of the heterodyning of the allowed and semiforbidden microwave transitions between the levels of a coupled electron-nuclear system (Fig. 1). For this to occur, both kinds of transitions must be excited simultaneously by the microwave transmitter pulses. If only one transition is induced, as is the case when the electron-nuclear coupling energy is much larger than the Zeeman energy, there is no modulation effect. There is also no modulation effect if the microwave field H_1 in the pulses is too weak, since then only one or the other of the heterodyning transitions can be driven by the pulses. As a rough criterion, H_1 should exceed the distance (in Gauss) between the relevant allowed and semiforbidden transitions. Even then, unless H_1 substantially exceeds the minimum criterion, the depth of modulation, which is an important parameter in some of the experiments described here, may be smaller than that predicted by simple formulae.

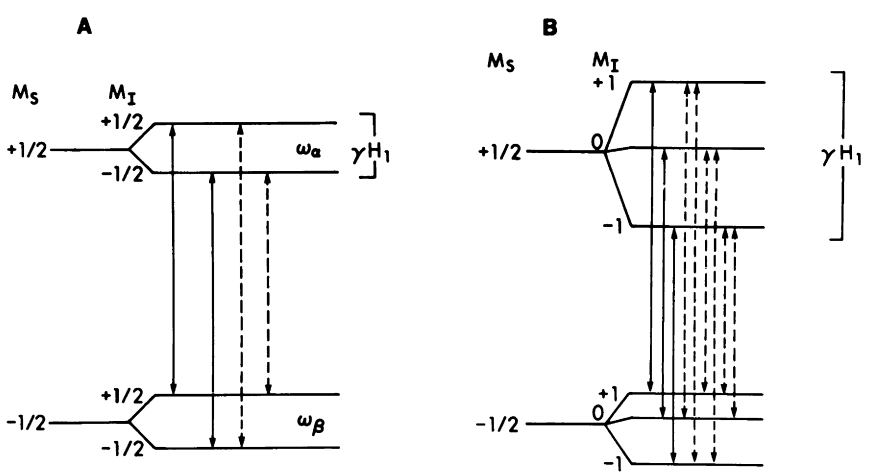

Fig. 1. A. Magnetic energy level scheme for an I = 1/2 nucleus coupled to an S = 1/2 electron spin. B. A level scheme for an I = 1 nucleus interacting with an S = 1/2 electron spin. Solid lines indicate allowed transitions; broken lines indicate semiforbidden transitions.

Two minor experimental points are worth noting. The description of the echo process in terms of 90° and 180° pulses, which is usually given in NMR texts, is largely irrelevant in the case of ESE experiments on frozen metalloprotein solution samples. The range of microwave excitation (~ $\pm H_1$ on either side of resonance) is usually much less than the width of the overall spectral distribution, so that during the microwave pulses, most spins are undergoing motions of a much more complex kind. Fortunately, this makes no major difference to the modulation pattern, provided that H_1 is large enough to excite both allowed and semiforbidden transitions in the same way for the systems falling within the $2H_1$ bandwidth. It has no effect on the observed modulation frequencies, which depend on nuclear precession occurring in the intervals between the pulses, although it can result in a small shift in the zero of the time scale, by an amount not exceeding half the transmitter pulse width.

A second practical point is that it does not usually matter if the echo repetition rate is too fast to allow complete relaxation between echo cycles. The echo signal amplitude will be reduced by the partial saturation of the spin system, but this disadvantage may be more than offset by the greater speed of data accumulation. Changes in the modulation depth could, in principle, be caused by differences in the relaxation rates of allowed and semiforbidden transitions, but any such effect is generally obscured by cross relaxation in samples having the usual paramagnetic concentrations. Only when non-cross-relaxing species are simultaneously excited is there some risk of observing a rate-dependent modulation effect.

Some final words of caution apply to the use of the simple theoretical formulae given below. These formulae assume that the two electron spin states involved in the resonance transition can be described by an effective spin S=1/2 and that the system has an isotropic g value. Envelope modulation is observed in many other cases, but the theoretical problem then becomes more complex. For instance, if the electron transitions are between the magnetic substates of the S = 5/2 Mn(II) ion, it may be necessary to diagonalize the whole 6 x 6 electron spin matrix in order to find the effective value of the electron magnetic moment M_z that enters into the calculation of the modulation frequencies and the modulation depth. Frequencies and depth may differ drastically from one Mn(II) electron transition to another. For a similar reason it is incorrect to apply the simple formulae given here to systems with a large g anisotropy, since in this case, M_z is not necessarily aligned parallel to the magnetic field H_0 and may be larger than the value one would calculate from the standard g formula (7). The modulation frequencies remain the same as the "ENDOR" frequencies for the system, but the calculation of these frequencies and of the modulation depth is less straight-

forward. This particular problem is often overlooked in biological experiments, and, indeed, the errors may not be large in comparison with those which result from spherical averaging together with any other convenient approximations. It should receive attention, though, if g is highly anisotropic and if modulation depth measurements play an important part in the interpretation of data.

2.1 Two-pulse echoes

When a nucleus with spin I = 1/2 is coupled with an electron with spin S = 1/2, and when g = 2, the envelope of two-pulse electron spin echoes (Fig. 2A) is modulated by a function:

$$V_{mod}(\tau) = 1 - k/2 + (k/2)[\cos(\omega_\alpha\tau) + \cos(\omega_\beta\tau) - (1/2)\cos(\omega_\alpha + \omega_\beta)\tau - (1/2)\cos(\omega_\alpha - \omega_\beta)\tau] \quad [2.1]$$

where ω_α ω_β are the superhyperfine (ENDOR) frequencies associated with the upper and lower electron spin states. If the electron nuclear coupling is purely dipolar, the modulation depth factor k is given by:

$$k = (\omega_I B/\omega_\alpha\omega_\beta)^2 \quad [2.2]$$

where $\omega_I = (1/\hbar)(g_n\beta_n H_0)$ [2.3]

and $B = (1/\hbar)(gg_n\beta\beta_n)(3\cos\theta\sin\theta)/r^3$. [2.4]

The quantities g, g_n, β, β_n, are the g factors and the values of the magneton for the electron and nucleus, H_0 is the Zeeman field, r is the distance between the electron and nucleus, and θ the angle between the line joining the electron and nucleus and H_0. In Eqn. 2.3 ω_I is the free precession frequency (in radian units) of the nucleus (i.e. the frequency that might be observed in the absence of any electron-nuclear coupling). The frequencies ω_α, ω_β are given (in the case of pure dipolar coupling) by:

$$\omega_\alpha^2 = (B/2)^2 + (A_d/2 + \omega_I)^2 \quad [2.5]$$

$$\omega_\beta^2 = (B/2)^2 + (A_d/2 - \omega_I)^2 \quad [2.6]$$

where

$$A_d = (1/\hbar)(gg_n\beta\beta_n)(3\cos^2\theta - 1)/r^3. \quad [2.7]$$

For proton modulation as commonly observed in an X-band ESEEM experiment, the dipolar coupling coefficients A_d and B are several times smaller than ω_I. Then, to the first order of approximation, $\omega_\alpha \simeq \omega_I + A_d/2$, $\omega_\beta \simeq \omega_I - A_d/2$, $k \simeq (B/\omega_I)^2$, and the modulation depth varies as $\sin^2(2\theta)/r^6$. The maximum modulation depth occurs at $\theta = 45°$, i.e. at an angle for which the A_d term is relatively small. The sum frequency term in Eqn. 2.1 is independent of A_d and reduces, in first order of approximation, to

$$-1/4k\cos(2\omega_I\tau). \quad [2.8]$$

Because of the variation of A_d with the orientation of the centers in a frozen solution sample the fundamental frequency term is spread out over a frequency band, and the corresponding modulation pattern is rapidly damped out.

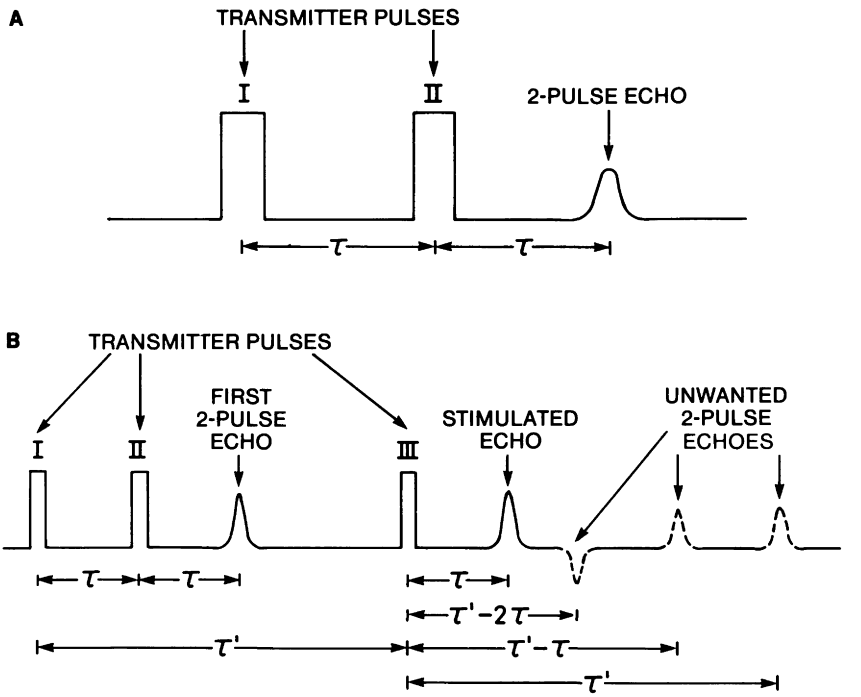

Fig. 2. (A) 2-pulse and (B) 3-pulse electron spin echo sequences In 2-pulse experiments, the echo envelope is obtained by gradually increasing τ in successive pulse sequences, the amplitudes being measured by sample hold circuitry. In 3-pulse studies, τ is set to a fixed value and τ' is varied. The "unwanted" two pulse echoes in B result from the failure of ideal 90-90 pulse conditions in broad line samples. They correspond to different 2-pulse combinations of I, II, III, and the first 2-pulse echo.

The modulation pattern due to the harmonic term in [2.8] persists for a longer time since it is not, to the first order, dependent on A_d.

A more elaborate calculation taking into account the nuclear quadrupolar interaction energy is generally needed for nuclei with I>1/2. However, if the nuclear quadrupolar energy is small compared with the Zeeman energy, it remains possible to use the I = 1/2 formulae with some modifications. This approximation can often be used in X-band experiments that involve coupling with molecules containing deuterium (I = 1), or that involve coupling with other nuclei such as ^{23}Na (I = 3/2) in environments that minimize the effects of nuclear quadrupolar coupling. The case of deuterium is of special importance in experiments aimed at investigating the accessibility of enzyme active sites to solvents and in substrate labelling experiments.

To the first order of approximation the four ENDOR transition frequencies

for weakly coupled deuterium nuclei are given in radian units by

$$\omega_1 = \omega_D + 1/2\ A_d + \omega_Q$$
$$\omega_2 = \omega_D + 1/2\ A_d - \omega_Q$$
$$\omega_3 = \omega_D - 1/2\ A_d + \omega_Q$$
$$\omega_4 = \omega_D - 1/2\ A_d - \omega_Q \qquad [2.9]$$

where $\omega_D = g_n\beta_n H_o/\hbar$ is the free nuclear precession frequency for deuterium nuclei (without dipolar or quadrupolar coupling),

$$A_d = (1/\hbar)gg_n\beta\beta_n(3\cos^2\theta - 1)/r^3 \qquad [2.10]$$

and where

$$\omega_Q=(3/8)e^2qQ(3\cos^2\theta_Q - 1)/\hbar. \qquad [2.11]$$

For D_2O, (which will serve as a model for the purposes of this discussion), the quadrupolar field is very nearly axial; θ_Q is the angle between the quadrupolar axis and H_o, and the zero field nuclear quadrupolar frequencies υ^+ and υ^- (in Hz units) are approximately given by

$$\upsilon^+ = \upsilon^- = (3/4)e^2Qq/h. \qquad [2.12]$$

The modulation depth parameter k_D for deuterium is 8/3 times that for protons, as prescribed by the formula: $k \alpha I(I + 1)$ (8-10). This formula holds good when the quadrupolar interaction is small compared with the Zeeman interaction, so that, for the initial part of the modulation pattern at least, the frequencies ω_1, ω_2, ω_3, ω_4 in Eqn. 2.9 can all be considered together, i.e. in this case approximated by ω_D. A detailed calculation for the $I = 1$ case also yields a number of terms in k_D^2 (11), which correspond to state mixing of the $M_I = \pm 1$ superhyperfine levels by the dipolar interaction. These terms result from the partial relaxation of the selection rule excluding the doubly forbidden $\delta M_I = 2$ nuclear quantum jump. However, they can be ignored in first order, leaving the simplified form of the two-pulse modulating function

$$V_{mod} = (1 - (1/2)k_D) + (1/4)k_D(\cos\omega_1\tau + \cos\omega_2\tau + \cos\omega_3\tau + \cos\omega_4\tau)$$
$$- (1/8)k_D[\cos((\omega_1 + \omega_3)\tau) + \cos((\omega_2 + \omega_4)\tau)$$
$$+ \cos((\omega_1 - \omega_3)\tau) + \cos((\omega_2 - \omega_4)\tau)]. \qquad [2.13]$$

As may be seen by substituting frequencies from Eqn. 2.9, the A_d term disappears in first order from the sum frequency terms, and ω_Q disappears from the difference frequency terms, leaving

$$V_{mod} = (1 - (1/2)k_D) + k_D\cos(\omega_D\tau)\cos((1/2)A_d\tau)\cos(\omega_Q\tau)$$
$$-(1/4)k_D\cos(2\omega_D\tau)\cos(2\omega_Q\tau) - (1/4)k_D\cos(A_d\tau). \qquad [2.14]$$

These formulae are easily extended to the case where the electron-nuclear spin Hamiltonian includes a small Fermi contact term of the form $A_c\underline{I}\cdot\underline{S}$. In Eqn. 2.9, ω_1 and ω_2 are increased by $(1/2)A_c$ whereas ω_3 and ω_4 are reduced by $(1/2)A_c$. The factors $\cos((1/2)A_d\tau)$, $\cos(A_d\tau)$ in Eqn. 2.14 become, respectively, $\cos((1/2)((A_c + A_d)\tau)$, $\cos((A_c + A_d)\tau)$.

Metal ion centers in proteins are surrounded by numerous weakly coupled

hydrogen atoms, and often also by other magnetic nuclei such as ^{14}N. All of these nuclei contribute simultaneously to the modulation pattern. If nuclei I_1, I_2, ...I_n are coupled to the same electron spin, then the overall modulation function is given by the product of the individual modulating functions, as indicated by the formula

$$V_N(I_1,I_2,...I_n) = V_1(I_1) \times V_2(I_2) \times ...V_n(I_n). \quad [2.15]$$

When the overall modulation depth in a particular experiment is not too great, it may be simpler to replace the product by the sum obtained by expanding the $V_r(I_r)$ terms Eqn. 2.15 to the first order in the individual depth parameters k_r. This linear approximation is sometimes a convenient way of representing the modulation function due to coupled nuclei that lie outside of the first coordination sphere. But caution is required when treating large numbers of nuclei, since the accumulation of higher order products $k_q k_r$ will eventually offset the smallness of the products considered individually. Higher order product terms may also include useful structural information as shown in section 2.9.

There are two disadvantages of the two-pulse ESEEM method relative to ENDOR. As can be seen from Eqns. 2.1 and 2.13 the function V_{mod} contains sum and difference frequency terms as well as terms in the individual superhyperfine frequencies. These sum and difference terms occur to the first order in the depth parameter k, and, although they are distinguished by their negative phase, and appear as distinct inverted lines in the cosine Fourier transform (see e.g., Fig. 9B) they can become a source of confusion in complex spectra. A second major disadvantage of the two-pulse ESEEM method is the shortness of the phase memory time, and the associated broadening of the superhyperfine lines that make the spectrum much harder to resolve than an ENDOR spectrum. In organic samples the phase memory time cannot be increased very much beyond $\simeq$ 2 microsec, either by lowering the temperature or by reducing the concentration of paramagnetic centers, since it is due to internal magnetic field fluctuations caused by spin-spin flips of hydrogen nuclei. These flips occur at a rate that, in the liquid helium range, is virtually independent of temperature. On the other hand, there are certain advantages of the ESEEM method. It allows one to detect electron-nuclear coupling for weakly coupled nuclei or for nuclei with very small moments, and it provides, via the modulation depth, an additional source of information. The insensitivity to the magnitude of the nuclear moment can be seen by setting $\omega_\alpha \simeq \omega_\beta \simeq \omega_I$ in Eqn. 2.2 and substituting values from Eqns. 2.3 and 2.4. The way in which modulation depth depends on the electron-nuclear coupling can be seen from Eqns. 2.2 - 2.4. The modulation depth is independent of instrumental settings, provided that the pulsed microwave transmitter can deliver adequate power, and generate the H_1 required in order to excite all the rele-

vant allowed and semiforbidden transitions.

Fortunately, it is possible to retain the advantages of the ESEEM method and avoid the disadvantages associated with two-pulse ESEEM experiments by performing experiments in the three-pulse "stimulated echo" mode. Although much of the early work was done in the two-pulse mode, it has subsequently been found that, in many instances, it is preferable to use the three-pulse method for metalloprotein studies. The two-pulse method is mainly useful for making a rapid check on the quality of a sample, and for obtaining a rough preview of its modulation properties before resorting to a more detailed and time consuming three-pulse study.

2.2 Three-pulse echoes

Under the conditions stated in conjunction with Eqn. 2.1, the modulating function in the three pulse case (see Fig. 2B) is given by

$$V_{mod} = 1 - (1/2)k\{\sin^2(\omega_\alpha\tau/2)[1-\cos(\omega_\beta\tau')] + \sin^2(\omega_\beta\tau/2)[1-\cos(\omega_\alpha\tau')]\} \quad [2.16]$$

where τ is the time between pulses I and II, τ' is the time between pulses I and III and the other quantities are as defined in the two-pulse case. The echo, often described as a "stimulated echo", appears at a time τ after pulse III.

The stimulated echo signal is, in fact, a form of free induction signal. The first two pulses, which in the idealized narrow-line case are 90° pulses, produce a toothed pattern in the resonance line (i.e. a toothed pattern in M_z, the z component of electron spin magnetization; see e.g., Fig. 12 in ref. 4). How this pattern is generated can be seen as follows. Immediately after pulse II, the spins exactly on resonance with the microwave transmitter frequency are inverted. Spins whose frequencies lie $\pm \pi/\tau$ on either side of exact resonance precess by ± 180° between pulses I and II and are returned to the normal state by pulse II. Spins with frequencies $\pm 2\pi/\tau$ away from exact resonance precess by 360° between the pulses and are inverted, just like the spins on exact resonance. Spins offset by $\pm 3\pi/\tau$ are returned to the normal state, and so on. In the more realistic wide-line case, where ideal 90° spin nutations do not occur, and where spin reorientation follows less simple rules, a toothed pattern of periodicity $2\pi/\tau$ in the frequency domain is still generated, but the pattern becomes shallower to either side of resonance, the principal effect being limited to a range $\pm 2H_1$. Because of the deviations from precise 90° spin nutation, there is some residual M_x and M_y magnetization, which results in precessional coherence and causes the appearance of a two-pulse echo at time τ after pulse II (see Fig. 2B) but this extra echo can be ignored for the moment. The important property of the toothed pattern in M_z is that it can persist for times that are very much longer than the phase memory time. Eventually it is erased by cross relaxation or by lattice

relaxation, but it can last as long as 100 μseconds in magnetically dilute samples at helium temperatures, even for those materials that contain large numbers of hydrogen nuclei. The actual lifetime of the pattern depends in part, on the value chosen for τ. Thus, the longer the time τ, the closer the teeth, and the more easily the M_z pattern is erased by cross relaxation.

The toothed pattern in M_z could, in principle, be measured by continuous wave EPR, using a rapid field sweep after pulse II, but it is easier to use the free induction technique. A third 90° pulse generates the Fourier transform of the M_z pattern, which consists of a pulse offset from pulse III by time τ. This is the stimulated echo. One can see as follows that this echo, like the two-pulse echo, varies in amplitude according to the nuclear modulation effect. Between pulses II and III the precession of nuclei, which are polarized by the sudden changes in local field caused by pulses I and II, produces cyclic variations in the local magnetic field acting on the electron spins. So, depending on the point reached in the nuclear precession cycle when pulse III is applied, the toothed pattern is either fully resolved or partially blurred in comparison with what it would be without any nuclear coupling. The stimulated echo amplitude thus varies according to the nuclear precession period and the pulse II to pulse III timing. The important difference between this and the modulation effect in two-pulse experiments is that the modulation patterns can now extend over many nuclear cycles, being limited only by the widths of the associated superhyperfine lines and not by the electron spin echo phase memory.

A further advantage of working in the three-pulse rather than the two-pulse mode will be apparent from Eqn. 2.16. If the experiment is conducted by setting τ to a constant value and by varying τ', then only the frequencies ω_α, ω_β, and not their sums or differences, appear in the result. However, the two frequencies ω_α and ω_β are not fully independent of one another, but are connected in a way that enables one to correlate them. For example, if one sets τ so that it comprises a whole number of cycles of the frequency ω_α, then ω_β is excluded from the envelope and vice versa. This "suppression effect", in which the frequencies belonging to the upper set of levels (M_S = + 1/2) are controlled by the frequencies belonging to the lower set (M_S = -1/2) and vice versa, also occurs with $I > 1/2$. Although in this case frequency suppression may only be partial, it is sometimes useful for deciding when two superhyperfine transitions occupy corresponding places in the upper and lower manifolds of superhyperfine levels (see e.g., Fig. 14 in ref. 4). The suppression effect is also useful for eliminating proton modulation when, as often happens in biological studies, this is of no particular experimental interest.

The product formula corresponding to Eqn. 2.15 for the three-pulse case

(12) is

$$V_{mod}(I_1,I_2,\ldots I_n) = (1/2)\prod_{i=1}^{n} V_i(\tau,\tau') + (1/2)\prod_{i=1}^{n} V_i(\tau',\tau) \qquad [2.17]$$

where $\prod$ is the product operator and the functions V_i are obtained by writing $V_{mod}(\tau,\tau')$ as the sum of two terms

$$V_{mod}(\tau,\tau') = (1/2)[V(\tau,\tau') + V(\tau',\tau)]. \qquad [2.18]$$

For instance, in Eqn. 2.16 V_{mod} can be written in the form [2.18] with $V(\tau,\tau')$ given by

$$V(\tau,\tau') = 1 - (1/2)k[1-\cos(\omega_\alpha\tau)][1-\cos(\omega_\beta\tau')]. \qquad [2.19]$$

If the electron is coupled with a nucleus with I>1/2 it is generally necessary to compute the three-pulse ESEEM function numerically (though if only the frequencies and not the modulation depths are required, an ENDOR type calculation is sufficient). However, some simplification can be made in the case of deuterium because of the small nuclear quadrupolar energies encountered in most deuterium-containing molecules. Assuming that the dipolar interaction, the quadrupolar interaction, and any contact interaction are all small in relation to the Zeeman energy, we can, as in the two-pulse case, write down first order expressions for the four ENDOR frequencies, and treat the modulation depth as being governed by a parameter k_D which is 8/3 larger than the parameter k in Eqn. 2.2. Terms in k_D^2 (i.e. terms involving $\delta M_z = 2$ transitions) can be ignored, and we have

$$\begin{aligned} V_{mod}(\tau,\tau') = 1 - (1/4)k_D([&\sin^2(\omega_1\tau/2)][1-\cos(\omega_3\tau')] \\ &+ [\sin^2(\omega_2\tau/2)][1-\cos(\omega_4\tau')] \\ &+ [\sin^2(\omega_3\tau/2)][1-\cos(\omega_1\tau')] \\ &+ [\sin^2(\omega_4\tau/2)][1-\cos(\omega_2\tau')]). \end{aligned} \qquad [2.20]$$

If the time τ is set to one deuterium cycle or less, it is often possible to approximate ω_1, ω_2, ω_3, $\omega_4 \simeq \omega_D$ in the $\sin^2(\omega\tau/2)$ factors, thus simplifying [2.20] still further. (See section 2.5.)

2.3 Application of formulae to frozen solution samples:Spherical averaging

It should be remembered that the formulae given in the previous sections of this article all refer to single crystal samples, in which the dipolar parameters A_d, B, the quadrupolar parameters υ_Q,θ_Q, etc., have specific values depending on the orientation of the molecules in the complex with respect to H_0. Before these formulae can be used to interpret data obtained with frozen solution samples, it is necessary to form a suitable average over all the orientations of the complex that contribute to the echo signal at a particular selected value of H_0 in the EPR spectrum. If all the relevant information were to be available, this average would be readily obtained by computation. More commonly, however, the problem presents itself in the in-

verse form. Very little is known at the outset, and the parameters have, for the most part, to be inferred by fitting computations based on sets of trial values to the experimental results.

Fortunately, it is possible to simplify the inverse problem by making some fairly coarse approximations. One of the most useful of these is to assume that the directions of the electron-nuclear line, and of the principal quadrupolar axes, are spherically distributed and uncorrelated with one another. Thus, for instance, in the case of a frozen solution of a paramagnetic ion in H_2O it may be assumed that the angle θ in Eqns. 2.4 and 2.7 takes on all values from 0° to 180°, and that a summation of computed echo envelopes, weighted by the spherical factor $\sin\theta$, will provide a curve that is good enough for comparison with experimental data. For the same complex in D_2O a double summation, incorporating a summation over θ and a second summation over θ_Q, the latter weighted by $\sin\theta_Q$, must be made. Where the modulation pattern is due to ^{14}N, an even coarser approximation has been found useful in some situations. The factor governing the depth of modulation is simply ignored, and a spherically averaged ENDOR frequency spectrum is computed without it. This spectrum has been found helpful in assigning ^{14}N transitions, although, since the amplitude values are incorrect, it cannot be transformed into a time wave to be compared with the echo envelope itself. A spherical averaging approximation is also useful when applying the product formula [2.15]. It is assumed here that the angular coordinates of each nucleus are uncorrelated with each other, so that the echo envelope in the multinuclear case can be found by multiplying the spherically averaged envelopes for each nucleus considered separately.

Of course, approximations such as these should be tested whenever possible by comparing the results of the calculation with experimental data on well characterized complexes, or by comparing the computations with others made at higher levels of sophistication. It should also be remembered that in using the spherical approximation one may sacrifice useful experimental information. By making measurements at a number of different H_0 settings one can work in an intermediate realm, somewhere between single crystal spectroscopy and spherically averaged frozen solution spectroscopy. For example, in the limiting case, one can approximate to single crystal conditions, by setting H_0 at the g_{max} or g_{min} ends of the frozen solution spectrum of a center with 3 different principal g values. Analyses along these lines have proved useful in ENDOR experiments, and are being tried out in ESEEM experiments.

When computing the frozen solution modulation pattern for deuterium, one can avoid lengthy simulations and take a short cut that involves the assumption that the angles θ and θ_Q are uncorrelated. The rationale of this pro-

cedure is as follows. We assume that the magnetic dipolar interaction and the quadrupolar interaction are both small in relation to the Zeeman energy so that the ENDOR frequencies can be approximated to the first order as in Eqn. 2.9. If there is, in addition, a small contact interaction of the form $A_c \underline{I}\cdot\underline{S}$ this can be included by adding a further first order correction of $+(1/2)A_c$ to ω_1,ω_2 and $-(1/2)A_c$ to ω_3,ω_4. Let us suppose that envelope simulations that take everything except the quadrupolar interaction into account, have already been made. Then the effect of introducing the terms $\pm\omega_Q$ in Eqn. 2.9 is to spread each monochromatic element in the frequency spectrum that corresponds to these simulations (other than the d.c. term) into a spectrum described by the function (13)

$\phi_Q(f) = \phi_{Q1}(f) + \phi_{Q2}(f)$

where

$\phi_{Q1}(f) = 1/(0.5\upsilon^{\pm}\text{-}f)^{1/2}$; ($f = -\upsilon^{\pm}$ to $0.5\upsilon^{\pm}$, $\phi_{Q1} = 0$ elsewhere),

$\phi_{Q2}(f) = 1/(0.5\upsilon^{\pm} + f)^{1/2}$; ($f = -0.5\upsilon^{\pm}$ to $\upsilon^{\pm}$, $\phi_{Q2} = 0$ elsewhere), [2.21]

and $\upsilon^{\pm} \simeq \upsilon^{+} \simeq \upsilon^{-}$ as in Eqn. 2.12.

This convolution of functions in the frequency domain becomes a multiplication in the time domain. The existing simulations can therefore be converted into simulations that include the deuterium quadrupolar interaction by multiplying them by the Fourier transform of $\phi_Q(f)$, which is denoted in the following discussion by $D_Q(t)$. Moreover, since ω_Q is not dependent on the electron nuclear distance r, the multiplication need only be performed once, on the products of the time waves for all similarly bonded (e.g. D_2O) deuterons in the problem. The required multiplying function $D_Q(t)$ is shown in Fig. 3. For deuterated ice this function crosses zero at $\simeq$ 4.2 μseconds and again at $\simeq$ 10.8 μseconds; between these two times the quadrupolar interaction causes a phase reversal in the deuteron modulation pattern.

The short cut method outlined above can be applied without further modification to three-pulse envelope computations. (The effect of introducing ω_Q into the $\sin^2(\omega_i\tau/2)$ factors in Eqn. 2.20 is small enough to be ignored if, as in many experiments, τ is set to a constant value of approximately half a deuterium cycle.) Two-pulse experiments involve an additional complication since the sum and difference terms give rise to distributions centered on zero frequency and on the second harmonic of the NMR frequency. The quadrupolar contribution cancels out for the former and is doubled for the latter (see Eqn. 2.14). The component in the time waveform corresponding to the very low frequency distribution is therefore unaffected by the introduction of the deuterium quadrupolar interactions, whereas the time waveform corresponding to the second harmonic must be multiplied by the function in Fig. 3 with time in units of $1/\upsilon\pm$ instead of $2/\upsilon\pm$ on the horizontal scale. This explains a frequently noted difference between two-pulse ^1H and ^2H

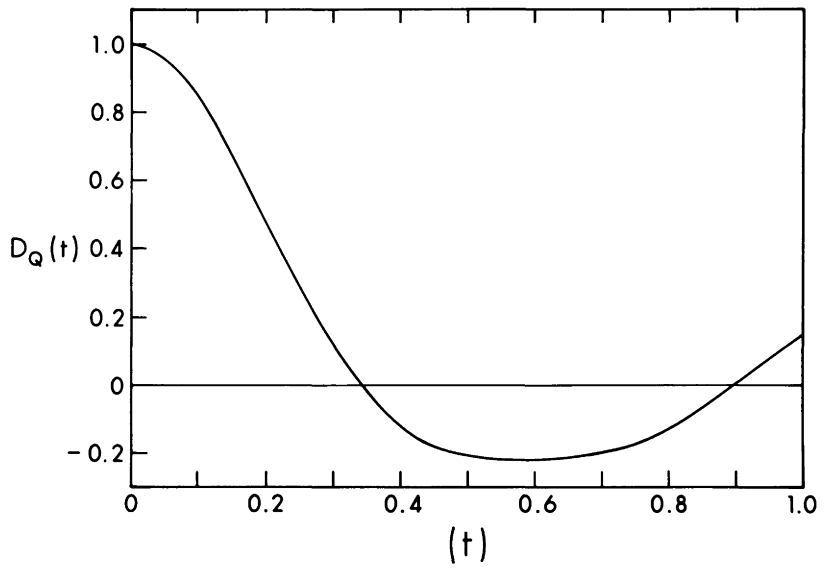

Fig. 3. A 3-pulse deuterium ESEEM pattern, computed without taking the nuclear quadrupolar interaction into account, can be converted into one which includes the nuclear quadrupolar interaction by multiplying it by $D_Q(t)$. (The d.c. term and other modulating functions that do not involve deuterium must first be removed.) Time is in units of $2/\upsilon\pm$ where $\upsilon\pm \simeq \upsilon+ \simeq \upsilon-$ (the quadrupolar field is assumed to be roughly axial). For deuterium in deuterated ice the graph covers times from 0 to approximately 12 microseconds.

modulation patterns. After a certain number of cycles ^1H patterns tend to be dominated by the second harmonic frequency, since the broadening effect of the dipolar interaction is absent for this harmonic component [see Eqn. 2.8]. But, in the case of ^2H patterns, both harmonics are broadened by the quadrupolar frequency offsets, the decay for the second harmonic being twice as fast as for the fundamental, so that there is no longer a tendency for the second harmonic to prevail at later times in the two-pulse envelope. Only if A_d or A_c are large do they become the major determinants and cause the ^1H type of modulation pattern to be seen in a deuterated sample.

2.4 Isotopic labelling and the method of waveform division

As pointed out earlier, the ESEEM method is especially useful for detecting nuclei that are weakly coupled to an electron spin. This suggests applications in which a substrate molecule is labelled with a nucleus such as ^2H or ^{13}C, so that the substrate to enzyme bonding can be studied by observing the magnetic interactions between the labelling nucleus and the metal ion at the enzyme active site. The problem is to disentangle the ESEEM component due to the nucleus in question from components due to all the other nuclei

present.

As an introductory illustration we cite an early experiment in which the binding between the metalloprotein complex Cu(II)-conalbumin and ^{13}C labelled oxalate anion was studied in this way (14) (Fig. 4A). The measurements were done in the two-pulse mode, though later experience suggests that a three-pulse study would probably have yielded better data and been more informative. Two two-pulse envelopes were recorded, one for Cu(II) conalbumin bound by normal C^{12} oxalate and one for Cu(II) conalbumin bound by ^{13}C-labelled oxalate. Certain minor differences between these two envelopes could, with some difficulty, be detected, but both patterns were dominated by modulation due to protons and due to ^{14}N nuclei belonging to an imidazole ligand (see section 2.7).

In order to enhance these small differences the echo envelope obtained with the ^{13}C-labelled oxalate was divided by the envelope obtained with the normal C^{12} oxalate (Fig. 4B). If the samples had been single crystals,

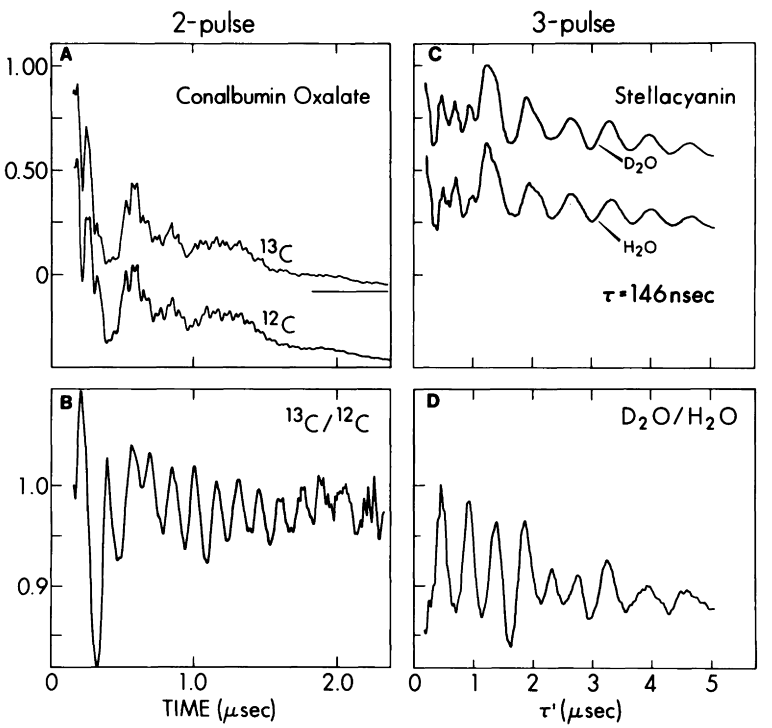

Fig. 4. A. ESEEM patterns for Cu(II) conalbumin with ^{13}C- and ^{12}C-oxalate. B. Ratio of envelopes in A. C. ESEEM patterns for stellacyanin in D_2O and H_2O. D. Ratio of envelopes in C.

then, according to Eqn. 2.15, one would in this way have factored out all the modulation components due to the ^{1}H and ^{14}N nuclei, since these nuclei were present in both samples alike, and the quotient waveform would have contained only those $V_i(I_i)$ components associated with the ^{13}C nuclei in oxalate. For the frozen solution samples that were actually used, this simple conclusion does not necessarily follow, however. Each of the two envelope measurements corresponded to an average over complexes with many different orientations, and the effect of the division was to give the quotient of the two averages. This is not the same thing as the average of the quotient waveforms for each orientation of the complex considered separately. In practice, however, the envelope-dividing procedure turned out to be reasonably successful in removing modulation due to ^{1}H and ^{14}N nuclei, and in revealing the ESEEM component due to ^{13}C. In spite of the smallness of the ^{13}C contribution in the two pulse envelope, it was easily established that oxalate was closely bound to the metal ion in Cu(II)-conalbumin.

More recently, studies of the same type were carried out with VO^{2+} pyruvate kinase using specifically labelled pyruvate to establish that both carbons 1 and 2 of the substrate are bound to the metal ion (15). Here contact interactions arising from each ^{13}C atom were observed, clearly demonstrating metal ligation.

The envelope dividing technique was further explored in some experiments on the heme-iron center in met-myoglobin (16). Three-pulse envelopes were measured for a sample prepared in a normal aqueous medium, and for a sample that had been exchanged against D_2O. Again, only minor differences were seen in the envelopes themselves, the modulation pattern being dominated by ^{14}N interactions from the heme and imidazole ligands, but the quotient envelope clearly showed a periodicity at $\simeq$2 MHz, i.e. at the frequency to be expected for weakly coupled deuterium nuclei. However, in this experiment the quotient envelope was not a simple cosine wave. Fourier transformation (Fig. 5) revealed a spectrum with three closely spaced peaks, a central peak at the frequency for weakly coupled deuterium, and two flanking peaks due to deuterium nuclei coupled via a small $A_c\underline{I}\cdot\underline{S}$ term. The flanking peaks were assigned to a water molecule directly coordinated to the Fe(III) ion in met-myoglobin, and the central peak to other deuterium nuclei, either replacing exchangeable hydrogen in the protein or occurring in ambient water.

Since the substrate labelling technique is likely to find numerous applications in metalloprotein studies, we note here some experimental requirements. First, it is desirable to make the measurements on the labelled and unlabelled materials under conditions that are as nearly identical as possible. Various minor errors, due to insufficient H_1 fields, decay of the three-pulse echo amplitude because of cross relaxation effects, etc., will

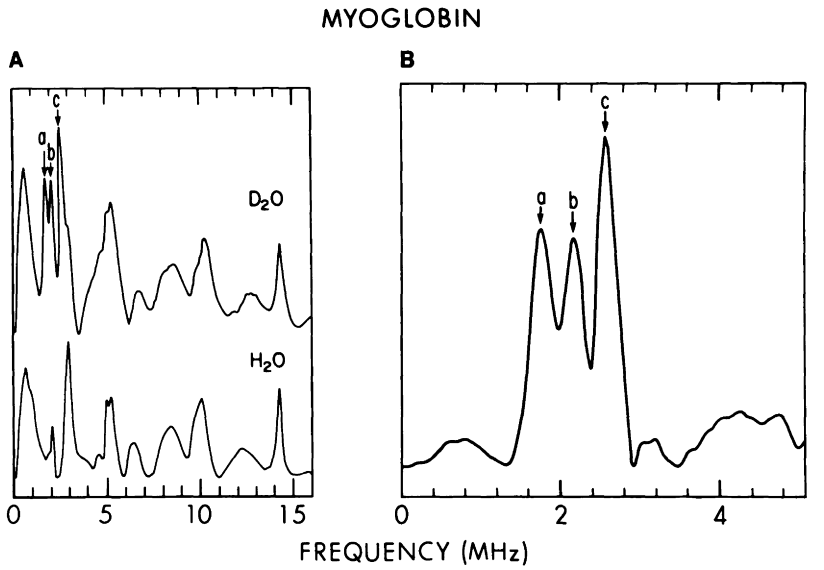

Fig. 5. (A). Cosine Fourier transform of the echo envelopes for metmyoglobin in D_2O (upper trace) and in H_2O (lower trace). Differences can be seen in the D_2O spectrum in the vicinity of 2 MHz. (B). Spectrum obtained by Fourier transforming the quotient of time wave forms for metmyoglobin in D_2O and in H_2O. Lines due to ^{14}N and ^{1}H are greatly reduced in intensity in the quotient spectrum. Peaks a and c are due to ^{2}H on a water molecule directly coordinated to heme Fe(III). Peak b is due to other weakly coordinated deuterium atoms.

then tend to cancel in the quotient. It is also important to have reliable baseline measurements. (This would matter less if one were simply making a subtraction instead of calculating a quotient.) The baseline can be recorded, together with each modulation tracing, by programming the ESE spectrometer so that the boxcar gate is moved off the echo signal for the last few percent of the envelope recording (see e.g., Figs. 11,12). Proton modulation can be eliminated by filtering e.g. by applying a Gaussian notch filter to the transformed envelope. But, it is better to eliminate as much of the proton modulation as possible by setting τ (in a three-pulse experiment) to a multiple of the proton period, thus using the suppression effect [see Eqn. 2.16]. This is not merely an alternative way of filtering the waveform. By suppressing proton modulation one (ideally) leaves the echo amplitude unaffected, whereas filtering leaves it reduced by half the proton depth parameter.

Although it can be shown to follow from the fundamental ESEEM formulae, the necessity for dividing time waveforms rather than subtracting frequency

spectra (i.e., taking 'difference spectra') may not be physically obvious. The product of the individual ESEEM waveforms contains, in addition to the individual nuclear frequencies, harmonics and combination frequencies (see Section 2.9) that are factored out, more or less successfully, by the waveform dividing procedure. These harmonics and combination frequencies correspond to what might be described as semi-semiforbidden microwave transitions, i.e., transitions that involve the flip of more than one coupled nucleus (see e.g., Fig. 5 in Ref. 17). If the modulation is very shallow, then the semi-forbidden transitions are already quite weak, and the semi-semiforbidden transitions can be ignored. In this case there is no distinction between the 'difference spectrum' and the spectrum obtained by transforming the quotient of two time waveforms.

2.5 Deuterium labelling and the measurement of electron nuclear distances

In the metmyoglobin experiment illustrated in Fig. 5 the presence of a contact interaction, implying some degree of covalent bonding, established that the water molecule was directly coordinated with Fe(III). Often, however, there is no measurable contact interaction for hydrogen or for deuterium in a ligating or substrate molecule. If the magnetic dipolar interaction were large enough, the frequency offsets due to A_d might be used to establish proximity and to estimate the nuclear distance (see Eqn. 2.7), but these offsets are often too small, and in frozen solution samples are distributed too smoothly over the spectrum to be reliably interpreted. The problem is worse for ESEEM than for ENDOR since the modulation depth, which depends on the factor $\sin^2 2\theta$, approaches zero for the angles θ=0 and θ=90 where the coefficient A_d reaches its extremal values. At the angle θ=50.8°, where the $\sin^2 2\theta$ factor weighted by the spherical factor $\sin\theta$ reaches its maximum, the $3\cos^2\theta$-1 factor in A_d has the value 0.2. Quadrupolar broadening tends to obscure the contribution due to A_d still further in the case of deuterium.

Fortunately, there is a good alternative method. Measurements may be made on the modulation depth, which is a more sensitive indicator of the electron-nuclear distance than A_d, since, for weakly coupled nuclei, it varies as $1/r^6$ (Eqns. 2.2, 2.4) rather than as $1/r^3$. For the best results and for simplicity of interpretation, experiments should be performed in the three-pulse mode with τ set equal to one half of the free deuterium nuclear precession period (i.e. $\tau \simeq 250$ nsec for X-band experiments). The deuterium modulation depth is then at or near its maximum value, the factors $\sin^2(\omega_i\tau/2)$ are effectively unity, and the small discrepancies between ω_1, ω_2, ω_3, ω_4 and ω_d only affect the result to the second order for the first few modulation cycles. Eqn. 2.20 becomes

$V_{mod}(\tau,\tau') \simeq 1-(1/4)k_D[4-\cos(\omega_1\tau')-\cos(\omega_2\tau')-\cos(\omega_3\tau')-\cos(\omega_4\tau')]$. [2.22]
(A correction factor, representing the spherical average of the deviations from unity of the factors $\sin^2(\omega_1\tau/2)$ etc., can easily be computed, but the errors introduced by omitting this factor are probably too small to matter in comparison with errors resulting from other approximations.)

The function V_{mod} might be simplified still further by setting $\omega_1,\omega_2,\omega_3,\omega_4$ to a common value ω_D in [2.22]. We then should have
$V_{mod}(\tau,\tau') \simeq 1-k_D(1-\cos\omega_D\tau')$ [2.23]
where substitution of the spherically averaged value
$k_D = (16/5)(g\beta/H_o)^2(1/r^6)$ [2.24]
in place of k_D would lead at once to the required value of r. (To obtain this mean value, approximate all frequencies to ω_D, apply the $k\alpha I(I+1)$ rule, and average over the sphere.) However, somewhat more care must be exercised in approximating the $\cos(\omega_i\tau')$ terms than in approximating the $\sin^2(\omega_i\tau/2)$ terms in [2.20], since τ' is usually several times longer than τ and the error is substantially larger. Errors which arise as a result of ignoring the quadrupolar interaction in [2.23] can be allowed for by applying a correction factor based on the spherical averaging assumption as in Fig. 3. It will be clear from this figure that there is a great advantage in making the measurement of modulation depth on the earliest available deuterium cycle. The size of the correction factor, and errors in the assumptions used to derive it, increase rapidly with time τ'. Measurements of modulation depth made on a single early cycle, or made on a least squares fit to this cycle, are likely to yield a more reliable result than a least squares fit to the whole of the deuterium modulation pattern.

The metmyoglobin result (Fig. 4) illustrates another problem often encountered in a deuterium labelling experiment. One peak in the spectrum obtained in this experiment was assigned to deuterons that did not belong to the D_2O molecule bound to the Fe(III) ion, but it was not possible to obtain any detailed structural information from the amplitude of this deuteron peak (i.e. from the depth of the associated modulation pattern), since it was not clear how many nuclei were involved. In the weakly coupled case, one nucleus at a small radial distance r modulates the envelope as deeply as several nuclei situated farther away. The modulation depth yields, in effect, the sum $\Sigma n_i r_i^6$ where n_i is the number of nuclei at distance r_i. Small displacements of the spectral line and observations of the accelerated decay of the modulation pattern, caused by the dipolar term A_d, offer an alternative means for estimating nuclear distances. But it is better to make measurements of this kind on protonated samples, free from the complications arising from the deuterium quadrupolar interaction.

In spite of these ambiguities, the sum $\Sigma n_i/r_i^6$ is often useful as

an indicator of the degree to which the metal ion active site is accessible to water or other components in the ambient medium, although the interpretation then depends on assumptions made about the form of the protein surface and should be supported by comparisons with model systems (18).

2.6 Problems arising from contact and pseudodipolar coupling

As pointed out earlier, the electron nuclear dipolar coupling must often be considered in conjunction with a contact coupling of the form $A_c\underline{I}\cdot\underline{S}$ when interpreting ESEEM data. In ^{13}C labelling experiments, such as the Cu(II)-conalbumin oxalate experiment used as an introductory example in section 2.4, and in experiments that involve the interpretation of ESEEM patterns due to ^{14}N and ^{15}N nuclei (see section 2.7), the observed contact term is often as large as the Zeeman term. In such cases, it is necessary to review the simple assumptions made hitherto.

The first and most obvious effect of a large contact term is to shift the nuclear frequencies. If the contact term is appreciable but still not as large as the Zeeman term, the ESEEM spectrum for an I=1/2 nucleus will contain two lines at approximately $g_n\beta_nH_0\pm(1/2)A_c$, as in the D_2O coordinated met-myoglobin experiment cited in section 2.5. If the contact term is of roughly the same order of magnitude as the Zeeman term, as in the Cu(II)-conalbumin oxalate experiment, one of the frequencies will be very low and may be hard to detect. If the contact term is comparable with, but larger than the Zeeman term, then there will be lines at approximately $(1/2)A_c\pm g_n\beta_nH_0$. When the contact term is very much larger than the Zeeman term, the modulation effect becomes shallow or vanishes altogether since, in this limit, the "allowed" transitions are almost 100% allowed, and the "semiforbidden" transitions are exceedingly weak (see the introduction to section 2).

A secondary effect of the shift in nuclear frequencies is to change the modulation depth. This can be seen from Eqn. 2.2. If, because of the contact interaction, one of the two frequencies $\omega_\alpha,\omega_\beta$ becomes very small, the depth factor k is much larger than it would be otherwise. But there is a different reason why the modulation depth may be anomalously large in cases such as this, and to understand the reason it is necessary to take into account the full expression for the electron-nuclear interaction.

The interaction associated with the partial covalency of a coordinating bond is described by the product $\underline{I}\cdot\underline{\underline{A}}\cdot\underline{S}$, where $\underline{I}$ is a vector made up of the nuclear spin operators I_x,I_y,I_z, $\underline{S}$ is a vector made up of the electron spin operators S_x,S_y,S_z, and $\underline{\underline{A}}$ is a 3 x 3 matrix containing the elements $A_{xx},A_{xy},A_{xz},A_{yx},A_{yy}$, etc. If the z axis is parallel to H_0, and if the electron spin is aligned along this axis (i.e., if H_0 is set at the g_z end of the EPR spectrum), the component $A_{zz}I_zS_z$ in

the expansion of $\underline{I}\cdot\underline{\underline{A}}\cdot\underline{S}$, together with the dipolar and Zeeman interactions determine (to the first order) the superhyperfine frequencies. The terms $A_{xz}I_xS_z$ and $A_{yz}I_yS_z$, together with terms of similar form in the dipolar interaction determine the modulation depth. If, however, H_0 is moved from the g_z end of the EPR spectrum to the g_x end, then the component $A_{xx}I_xS_x$ replaces $A_{zz}I_zS_z$ in the determination of the superhyperfine frequencies, and $A_{zx}I_zS_x$ together with $A_{yx}I_yS_x$ replace $A_{xz}I_xS_z$ and $A_{yz}I_yS_z$ in the determination of modulation depth. Changes of this kind are usually described by rotating the x,y,z axes to new axes x′,y′,z′. The interaction then becomes $\underline{I}'\cdot\underline{\underline{A}}'\cdot\underline{S}'$, where $\underline{I}',\underline{S}'$ are new spin operators, and where $\underline{\underline{A}}'$ is a matrix derived from $\underline{\underline{A}}$ by making a similarity transformation. Once the transformation of axes is made, it is convenient to drop the primes, remembering that the numbers in the $\underline{\underline{A}}$ matrix will be different after the transformation (i.e., after the rotation of H_0 relative to the principal g axis).

The contact term $A_c\underline{I}\cdot\underline{S}$ represents only a part of $\underline{I}\cdot\underline{\underline{A}}\cdot S$, the number A_c being 1/3 x the trace of the matrix A, i.e., $A_c = (1/3)(A_{xx}+A_{yy}+A_{zz})$. The $A_c\underline{I}\cdot\underline{S}$ term has the useful property that it remains unaltered when the axis system is rotated (i.e., when the H_0 setting is changed). In the case of the electron-nuclear coupling this contact term often accounts for most of the coupling energy. But, the residual term $\underline{I}\cdot\underline{\underline{A}}\cdot\underline{S} - A_c\underline{I}\cdot\underline{S}$ also contributes to the superhyperfine frequencies, and can cause line broadening, because of the inhomogeneous distribution of orientations, as well as shifts in the ENDOR line positions as the field H_0 is scanned from one end of the spectrum to another. Also important to note is that this term contains components $A_{xz}I_xS_z$ and $A_{yz}I_yS_z$ (i.e., modulation depth terms) that vary with the rotation of the axes (or with the H_0 setting), and which can outweigh the effect of the magnetic dipolar interaction, thus invalidating the formula for the coefficient B in equation 2.4. Together with the changes in the frequencies ω_α, ω_β caused by A_c, etc., these components of $\underline{\underline{A}}$ can radically modify the depth parameter k (see Eqns. 2.2 and 2.4), rendering it no longer a usable measure of the electron-nuclear distance r.

The residue $\underline{I}\cdot\underline{\underline{A}}\cdot\underline{S} - A_c\underline{I}\cdot\underline{S}$ is sometimes referred to as the "pseudodipolar coupling". This is an easily remembered name, but it should be noted that the pseudodipolar coupling involves covalency effects and is not merely an enhancement of the "classical" dipolar coupling used in deriving Eqns. 2.4, 2.7, etc. "Classical" dipolar coupling signifies the electron magnetic interaction between small bar magnets with centers a distance r apart. For low symmetry electron nuclear coupling geometries such as those that occur in metalloproteins, (for example, in the oxalate coordinated

Cu(II)-transferrin complex discussed in section 2.4, where coupling is transmitted from Cu(II) through oxygen to ^{13}C in the coordinated ligand) it is quite unlikely that the interaction has the simple cylindrical symmetry of the classical dipolar interaction. There is also no reason to suppose that the principal axes of $\underline{\underline{A}}$ and of the classical dipolar interaction are the same. In general, caution is needed when interpreting modulation depths for materials that show a sizeable $A_C\underline{I}\cdot\underline{S}$ term. This term may be symptomatic of the presence of a significant $\underline{I}\cdot\underline{\underline{A}}\cdot\underline{S}$ coupling, containing pseudo-dipolar elements that enhance (or possibly reduce) the modulation depth in unforeseeable ways. In order to fit the full $\underline{I}\cdot\underline{\underline{A}}\cdot\underline{S}$ to experimental data, 6 new variables are needed (5 in addition to A_C), and these still do not give the one structurally important quantity, namely the electron-nuclear distance.

Similar reservations apply to the interpretation of modulation depths due to other labelling nuclei, including deuterium. Fortunately, deuterium labelling often occurs at positions where the $\underline{I}\cdot\underline{\underline{A}}\cdot\underline{S}$ term is small compared with the Zeeman term, as evidenced by the lack of any large displacement of the NMR frequency. But ^{15}N, which often coordinates a metal ion directly, or which can occur in the structural backbone of a labelled molecule, tends to resemble ^{13}C in being subject to large $\underline{I}\cdot\underline{\underline{A}}\cdot\underline{S}$ couplings, equalling or exceeding the Zeeman energy (see section 2.8).

2.7 Coupling with nitrogen nuclei

The ^{14}N (I=1) nucleus has a quadrupole moment that, in many organic molecules, leads to zero field splittings which are comparable with the ^{14}N Zeeman energy encountered in X-band ESE experiments (0.92 MHz at 3000 G). There can also be a contact interaction of the same order of magnitude, e.g. for nitrogen directly coordinating Fe(III), or for nitrogen nuclei indirectly coordinating Cu(II) such as from bound imidazole. These different terms in the electron nuclear interaction may be separated and analyzed by substituting ^{15}N (I=1/2) for ^{14}N. The situation is then similar to that described for ^{13}C in the previous section. But more information can often be obtained from the nitrogen modulation pattern in unsubstituted material, in which it is possible, through the nuclear quadrupole parameters, to identify the ligand molecule chemically.

This can be illustrated by the much studied case of the Cu(II)-imidazole complex (19), which occurs in many copper proteins. Imidazole consists of a five membered ring containing two nitrogens and three carbons, the two nitrogens being separated by a carbon. The Cu(II) ion coordinates one nitrogen, the other, the "remote" nitrogen usually being protonated. The Cu(II):^{14}N interaction for the directly coordinating nitrogen is dominated by a large A term and cannot be observed by the ESEEM method (although it can be studied

by ENDOR). For the remote nitrogen the term A_C is (in X-band experiments) comparable in magnitude with the Zeeman interaction. The full $\underline{I}\cdot\underline{\underline{A}}\cdot\underline{S}$ term consists of a pseudodipolar component (see section 2.6), which enhances the modulation depth, so that the modulation is easy to observe in spite of the considerable electron nuclear distance (4.16 Å), and a contact term which, as will shortly appear, greatly facilitates the measurement of the ^{14}N quadrupolar parameters.

As was pointed out in the previous section, it is the component $A_{ZZ}S_ZI_Z$ in the spin Hamiltonian operator $\underline{I}\cdot\underline{\underline{A}}\cdot\underline{S}$ and not the contact term $A_C\underline{I}\cdot\underline{S}$ that concerns us here. However, if the value of $A_{ZZ}I_ZS_Z$ does not vary greatly as the z axis is rotated (i.e as the electron spin reorients itself in response to changes in the direction of H_0) then the effect on the superhyperfine frequencies is largely determined by the $A_C\underline{I}\cdot\underline{S}$ component in the electron nuclear interaction, and we can for convenience speak of the contact term, bearing in mind that, in careful measurements, it might become necessary to take the anisotropic part of $\underline{I}\cdot\underline{\underline{A}}\cdot\underline{S}$ into account.

In the case of the Cu(II)-imidazole complex the description in terms of a simple contact interaction will suffice for the purpose of the present discussion (Fig. 6). For the remote nitrogen of the imidazole ligand, in the protonated state, A_C has a value of approximately 2 MHz. The $M_S = +1/2$ superhyperfine states are therefore shifted up by 1 MHz, and the $M_S = -1/2$ states are shifted down by the same amount. For one set of states the $0.5A_C$ shift adds to the ^{14}N Zeeman component (0.92 MHz at 3000 G), and for the other set, it almost cancels the Zeeman component. The situation can be described in physical terms by saying that the A_C term generates a local magnetic field at the ^{14}N nucleus that roughly doubles the Zeeman field for one set of states and reduces the Zeeman field almost to zero for the other set. This results in an interesting situation. The energy levels for the latter set of superhyperfine states are almost the same as they would be in a zero-field nuclear quadrupole spectroscopy experiment, (if indeed, an experiment could be performed in the presence of the Cu(II) paramagnet).

In an experiment on the copper protein stellacyanin (Fig. 7), the frequencies obtained by Fourier transforming an experimental three-pulse echo envelope recorded at 3170 Gauss, were 0.7, 1.47 and 4.0 MHz (20). Of these the first two are close to the zero field quadrupolar frequencies υ^- and υ^+ for protonated imidazole, $(\upsilon^+, \upsilon^-, \upsilon^0) = (1.42, 0.72, 0.70)$. The high frequency corresponds to a transition between the $M_I = +1$ and $M_I = -1$ levels of ^{14}N in protonated imidazole in a field $H_0 \simeq 6000$ G, i.e. twice the Zeeman field. This accounts for all the ^{14}N ENDOR transitions except the two corresponding to $M_I = +1 \simeq 0$ and $M_I = -1 \simeq 0$ at the